THE JOURNAL OF CHEMICAL PHYSICS **125**, 084509 (2006)

Analysis of kinetic isotope effects for nonadiabatic reactions

Hyojoon Kim,[a] Gabriel Hanna,[b] and Raymond Kapral[c]
Chemical Physics Theory Group, Department of Chemistry, University of Toronto, Toronto, Ontario M5S 3H6, Canada

(Received 17 May 2006; accepted 21 July 2006; published online 28 August 2006)

Factors influencing the rates of quantum mechanical particle transfer reactions in many-body systems are discussed. The investigations are carried out on a simple model for a proton transfer reaction that captures generic features seen in more realistic models of condensed phase systems. The model involves a bistable quantum oscillator coupled to a one-dimensional double-well reaction coordinate, which is in turn coupled to a bath of harmonic oscillators. Reactive-flux correlation functions that involve quantum-classical Liouville dynamics for chemical species operators and quantum equilibrium sampling are used to estimate the reaction rates. Approximate analytical expressions for the quantum equilibrium structure are derived. Reaction rates are shown to be influenced significantly by both the quantum equilibrium structure and nonadiabatic dynamics. Nonadiabatic dynamical effects are found to play the major role in determining the magnitude of the kinetic isotope effect for the model transfer reaction. [DOI: 10.1063/1.2336778]

I. INTRODUCTION

Quantum mechanical reaction rates can be determined by evaluating time correlation functions of the fluxes of reactant and product chemical species.[1,2] The computation of such correlation functions involves sampling initial conditions from quantum equilibrium distributions and quantum time evolution of chemical species operators. Both the equilibrium and dynamical parts of the calculation present challenges for applications to condensed phase systems and a number of computational schemes have been proposed to compute the structure and dynamics.[3–22]

One of the signatures of quantum effects on the value of the reaction rate constant is the magnitude of the kinetic isotope effect. For instance, quantum effects on proton transfer rates in chemical and biological systems have been established through experimental measurements of the isotope effect when the proton is replaced by the deuteron.[23–25] The magnitude of the isotope effect is determined by contributions arising from the equilibrium structure, as reflected in the transition state theory value of the rate constant, and in dynamical effects that lead to deviations from transition state theory. The effect of nonadiabatic dynamics on the magnitude of the isotope effect has been a matter of some debate for realistic models of condensed phase proton transfer reactions.[26–34]

In order to explore some of these issues, we consider a model of a strongly bonded proton transfer reaction where the protonic degree of freedom is directly coupled to a single bath coordinate that serves as the reaction coordinate for the reaction. This reaction coordinate is, in turn, coupled to a harmonic many-body bath. This model, while highly idealized, captures generic features of real proton transfer reactions where functions of bath coordinates, such as the solvent polarization, can be used to monitor the progress of the reaction. For this simple model we can examine the various contributions to the isotope effect coming from equilibrium, adiabatic, and nonadiabatic effects.

In many circumstances quantum rates may be strongly nonadiabatic so that a description of the dynamics involving evolution on a single adiabatic surface is not adequate for an accurate estimation of the rate constant. Our description of the quantum dynamics is based on quantum-classical Liouville evolution[35–37] and we derive approximations to the quantum equilibrium structure that incorporate nonadiabatic effects.[38–42]

The paper is organized as follows: Section II gives the quantum-classical expression for the reaction rate coefficient on which our simulations are based and describes the simple quantum particle transfer model. The results of the calculations and a discussion of various contributions to the kinetic isotope effect are presented in Sec. III, while the concluding remarks are given in Sec. IV. The Appendix contains details of the derivation of the expression for the spectral density function that enters the reactive-flux correlation expression for the rate.

II. RATE COEFFICIENT AND MODEL SYSTEM

Our investigations are based on an expression[40] for the time-dependent rate coefficient of a general interconversion reaction $A \rightleftharpoons B$ whose progress can be monitored through a reaction coordinate $\xi(R)$, which is a function of the bath coordinates:[43]

---

[a] Electronic mail: hkim@chem.utoronto.ca
[b] Electronic mail: ghanna@chem.utoronto.ca
[c] Electronic mail: rkapral@chem.utoronto.ca

$$k(t) = \frac{1}{n_A^{\mathrm{eq}}} \sum_{\alpha} \sum_{\alpha' \geq \alpha} (2 - \delta_{\alpha'\alpha}) \times \int dX \, \mathrm{Re}\left[N_B^{\alpha\alpha'}(X,t) W_A^{\alpha'\alpha}\left(X, \frac{i\hbar\beta}{2} \right) \right], \tag{1}$$

where the spectral density function is

$$\begin{aligned} W_A^{\alpha'\alpha}\left(X, \frac{i\hbar\beta}{2} \right) &= \frac{1}{(2\pi\hbar)^{2\nu} Z_Q} \int dX' \frac{P'}{M} \cdot \nabla_{R'} \xi(R') \delta(\xi(R') - \xi^{\ddagger}) \\ &\times \int dZ dZ' e^{-(i/\hbar)(P\cdot Z + P'\cdot Z')} \langle \alpha' ; R | \\ &\times \left\langle R + \frac{Z}{2} \right| e^{-(\beta/2)\hat{H}} \left| R' - \frac{Z'}{2} \right\rangle \\ &\times \left\langle R' + \frac{Z'}{2} \right| e^{-(\beta/2)\hat{H}} \left| R - \frac{Z}{2} \right\rangle | \alpha ; R \rangle . \end{aligned} \tag{2}$$

Here the bath phase space variables are denoted by $X=(R,P)$, $Z_Q = Tr e^{-\beta\hat{H}}$ and $n_A^{\mathrm{eq}} Z_Q$ are the total and reactant partition functions, respectively, while ν denotes the coordinate space dimension and β is the inverse temperature. The species operator that characterizes the B metastable state is $\hat{N}_B = \theta(\xi(R) - \xi^{\ddagger})$, where θ is the Heaviside function. The metastable A species is defined in an analogous manner. The dividing surface that separates metastable A and B species is located at $\xi(R) = \xi^{\ddagger}$. The evolution of the species variable $N_B^{\alpha'\alpha}(X,t)$ is determined by the quantum-classical evolution operator.[35] The rate constant k can be determined from the plateau value of $k(t)$.[44] This rate coefficient expression was obtained by starting from the quantum mechanical expression for the reaction rate, making use of a partial Wigner representation of the system and taking the quantum-classical limit of the dynamics while retaining the full quantum equilibrium structure in the spectral density function W_A.[39,40] In the adiabatic limit, the rate coefficient reduces to

$$k^{\mathrm{ad}}(t) = \frac{1}{n_A^{\mathrm{eq}}} \sum_{\alpha} \int dX \, \mathrm{Re}\left[N_{B,\mathrm{ad}}^{\alpha\alpha}(X,t) W_A^{\alpha\alpha}\left(X, \frac{i\hbar\beta}{2} \right) \right], \tag{3}$$

where the evolution of $N_{B,\mathrm{ad}}^{\alpha\alpha}(X,t)$ is confined to single adiabatic surfaces and transitions between these surfaces are not allowed.

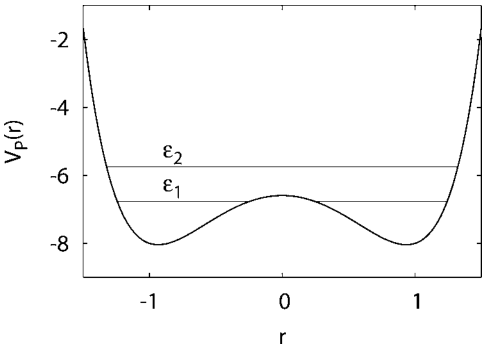

FIG. 1. Potential energy along the protonic coordinate r. The energies of the ground (ϵ_1) and first excited (ϵ_2) states of the proton are shown.

The partial Wigner transform of the Hamiltonian $\hat{H}$ of the system, $\hat{H}_W = P^2/2M + \hat{h}_W(R)$, where $\hat{h}_W(R)$ is the quantum subsystem Hamiltonian in the field of fixed bath particles, enters in the above formulation of the rate coefficient. Equation (1) is written in an adiabatic basis. The adiabatic eigenstates $\{|\alpha;R\rangle\}$ are the solutions of the eigenvalue problem $\hat{h}_W(R)|\alpha;R\rangle = E_\alpha(R)|\alpha;R\rangle$, where $\{E_\alpha\}$ are the adiabatic energies. The partially Wigner-transformed Hamiltonian of our model system is given by

$$\hat{H}_W = \frac{\hat{p}^2}{2m_H} + \hat{V}_P(\hat{r}) + \hbar\gamma'(R_0)\hat{r} + \frac{P_0^2}{2M_0} + V_n(R_0) + \sum_{j=1}^{\nu-1} \frac{P_j^2}{2M_j} + V_{b(n)}(R_b;R_0). \tag{4}$$

It describes a quantum system with Hamiltonian $\hat{H} = \hat{H}_{sn} + \hat{H}_{b(n)}$ composed of two bilinearly coupled nonlinear oscillators with coordinate and momentum operators $(\hat{r},\hat{p})$ and $(\hat{R}_0,\hat{P}_0)$ whose Hamiltonian is $\hat{H}_{sn}$, and a harmonic bath that is bilinearly coupled to the R_0 oscillator whose Hamiltonian in the field of the R_0 coordinate is $\hat{H}_{b(n)}$.

We take $(\hat{r},\hat{p})$ to represent the position and momentum operators of the proton with mass m_H. The potential energy of the proton is given by a double-well form that mimics the interaction of a proton in a strongly hydrogen bonded complex:

$$V_P(r) = D\{(1 - e^{-d(r+r_0)})^2 + (1 - e^{-d(r-r_0)})^2\} - 2D. \tag{5}$$

The two minima correspond to the metastable A and B states in the absence of coupling to the bath (see Fig. 1). This potential function can be generalized easily to treat asymmetric cases. The parameters $D=7$, $d=1.3$, and $r_0=1$ were chosen to correspond to a strong hydrogen bond.

The coupling of the R_0 oscillator to the proton is given by $\hbar\gamma'(R_0)\hat{r}$, where $\gamma'(R_0) = \gamma_0' R_0$ and γ_0' is a constant. The quartic oscillator with potential $V_n(R_0) = AR_0^4/4 - BR_0^2/2$ is bilinearly coupled to $\nu-1$ independent one-dimensional harmonic oscillators. The harmonic bath potential including the coupling to the quartic oscillator is given by $V_{b(n)}(R_b;R_0) = 1/2\sum_{j=1}^{\nu-1} M_j\omega_j^2(R_j - c_j\omega_j^{-2}M_j^{-1}R_0)^2$, where ω_j and M_j are the frequency and mass of the jth oscillator, respectively. The bilinear coupling is characterized by an Ohmic spectral density depending on the Kondo parameter ξ_K.[45] In this model we see that transitions between the two metastable wells of the R_0 quartic oscillator induce hops in the protonic subsystem that, in turn, influence the R_0 dynamics. Such coupling mimics the influence of solvent degrees of freedom on proton transfer in the condensed phase.

The Hamiltonian (4) may be written in the subsystem basis $\{|\alpha\rangle\}$, which is obtained by solving the Schrödinger equation for the isolated proton, $\hat{H}_P|\alpha\rangle = \epsilon_\alpha|\alpha\rangle$, where $\hat{H}_P = \hat{p}^2/2m_H + \hat{V}_P(\hat{r})$. In order to solve this eigenvalue problem, the wave function $|\alpha\rangle$ is expanded in a set of normalized basis functions, $|\alpha\rangle=\Sigma_i c_{i\alpha}|\varphi_i\rangle$, which are chosen to be the solutions of the quantum harmonic oscillator,

$$\varphi_i(r)=\langle r|\varphi_i\rangle=(2^n n!\sqrt{\pi})^{-1/2}b^{1/2}H_n(b(r-r_0)) \times\exp[-b^2(r-r_0)^2/2], \tag{6}$$

where n is an integer, $H_n(x)$ is a Hermite polynomial, and the index i on the basis function represents a pair of values (n,r_0). We use a total of 16 basis functions, consisting of two sets of eight functions $(n=0,\ldots,7)$ with $b=2$. One set is centered at $r_0=1$, and the other set at $r_0=-1$, the minima of the wells in the protonic potential. This leads to the standard eigenvalue problem, $Hc=Sc\epsilon$, where H is the Hamiltonian matrix with elements, $H_{ij}=\langle\varphi_i|\hat{\mathrm{H}}_P|\varphi_j\rangle$, and S is the overlap matrix with elements, $S_{ij}=\langle\varphi_i|\varphi_j\rangle$. The matrix elements $\{H_{ij}\}$ and $\{S_{ij}\}$ are evaluated numerically. The coefficients $\{c_{i\alpha}\}$ satisfy the normalization condition, $\Sigma_{ij}c_{i\alpha}S_{ij}c_{j\alpha}=1$. The eigenvalue problem is then solved to obtain $\{\epsilon_\alpha\}$ and $\{|\alpha\rangle\}$, from which we choose the lowest two states $\{|\alpha\rangle\}=|1\rangle,|2\rangle$ to form the basis for representing the system Hamiltonian.

The adiabatic states are obtained by diagonalization of the two-level Hamiltonian in the subsystem basis.[46] The corresponding adiabatic energies are given by

$$E_\alpha(R)=E_\alpha^{sn}(R_0)+V_{b(n)}(R_b;R_0), \tag{7}$$

where

$$E_\alpha^{sn}(R_0)=V_n(R_0)\mp\sqrt{\Omega^2+\gamma(R_0)^2}. \tag{8}$$

Here, $\gamma(R_0)=\gamma_0R_0$, $\gamma_0=\gamma'_0\langle 1|\hat{r}|2\rangle$, and $\Omega=(\epsilon_2-\epsilon_1)/2$. The factor γ'_0 is used to scale the magnitude of the coupling between the quantum particle and R_0 coordinate while the factor $\langle 1|\hat{r}|2\rangle$ is computed explicitly in order to correctly determine the relative magnitudes of the coupling for the proton and deuteron. The sign in Eq. (8) is negative for the ground state and positive for the excited state. For convenience, we have shifted the adiabatic energies by $-(\epsilon_1+\epsilon_2)/2$.

Sampling initial conditions for the calculation of the rate coefficient in Eq. (1) requires a knowledge of the spectral density function W_A. Since the expression for W_A derived previously[40] was restricted to weakly nonadiabatic systems, a more general expression for this quantity is needed. In common with many treatments of spin-boson-type systems, the derivation assumes that the imaginary time propagator is separable into system and bath parts,[6] $\exp(-\beta\hat{H}) \approx\exp(-\beta\hat{H}_{sn})\exp(-\beta\hat{H}_{b(n)})$. A symmetric decomposition of the propagator $e^{-\beta\hat{H}_{sn}}=e^{-\beta\hat{h}_{sn}/2}e^{-\beta P^2/(2M)}e^{-\beta\hat{h}_{sn}/2}+\mathcal{O}(\beta^3)$ is then used in the evaluation of the matrix elements. This approximation is useful for the treatment of condensed phase systems at high temperatures. The details of the calculation under these conditions for a general quantum subsystem and bath are given in the Appendix.

For the model system under study, R_0 is the only coordinate that directly couples to the protonic subsystem and we choose $\xi(R)=R_0$ as the reaction coordinate and $\xi^\ddagger=R_0^\ddagger=0$ for this symmetric system. In order to mimic situations where the proton transfer occurs in a solvent of massive molecules we consider a limiting situation where the bath degrees of freedom (R_0 oscillator and harmonic bath) are treated classically but the protonic system is treated quantum mechanically in W_A. This limiting form of the general expression for W_A is also given in the Appendix. For our two-level system, the result is

$$W_A^{\alpha'\alpha}\left(X,\frac{i\hbar\beta}{2}\right)=\frac{P_0}{M_0}\delta(R_0)\frac{e^{-\beta H_\alpha(X)}}{(2\pi\hbar)^\nu Z_Q}\{(1+D_\alpha)\delta_{\alpha'\alpha}+O_{\alpha'\alpha}\}. \tag{9}$$

Here $H_\alpha(X)=P^2/2M+E_\alpha(R)$ and the partition function is $Z_Q\approx(1/2\pi\hbar)^\nu\Sigma_\alpha\int dX\exp[-\beta H_\alpha(X)]$ in the high temperature limit. The functions D_α and $O_{\alpha'\alpha}$ contribute to the diagonal and off-diagonal terms, respectively, in the equilibrium spectral density.

The functions D_α and $O_{\alpha'\alpha}$ can be evaluated by numerical integration as discussed in the Appendix. They can also be determined analytically for high temperatures and weak enough coupling (see the Appendix) and the resulting forms provide insight into their structure. The diagonal contribution is given by

$$D_\alpha=\frac{1}{4\pi}\{\lambda_0^T d_{12}(0)\}^2(1-e^{(\beta/2)E_\alpha^{sn}(0)})^3, \tag{10}$$

with $d_{12}(0)=\gamma_0/(2\Omega)$ the nonadiabatic coupling matrix element at $R_0=0$ and $\lambda_0^T=(2\pi\beta\hbar^2/M_0)^{1/2}$ the thermal de Broglie wavelength corresponding to the R_0 degree of freedom. The off-diagonal contribution is

$$O_{\alpha'\alpha}=\frac{i}{4\pi}\{\lambda_0 d_{\alpha'\alpha}(0)\}e^{-(\beta/4)\{E_{\alpha'}^{sn}(0)+E_\alpha^{sn}(0)\}} \times(e^{-(\beta/4)E_{\alpha'}^{sn}(0)}-e^{-(\beta/4)E_\alpha^{sn}(0)})^2, \tag{11}$$

where $\lambda_0=2\pi\hbar/P_0$ is the de Broglie wavelength of the R_0 degree of freedom. Note that Eq. (11) satisfies the symmetry relation $O_{\alpha'\alpha}=O_{\alpha\alpha'}$. From these expressions we see that the magnitudes of D_α and $O_{\alpha\alpha'}$ depend on two factors: the first involves the change in the adiabatic wave function with R_0 over distances corresponding to λ_0^T and λ_0 for D_α and $O_{\alpha\alpha'}$, respectively, while the second involves the adiabatic energy evaluated at $R_0=0$. Note that $E_\alpha^{sn}(0)=\mp\Omega$. The sign of D_α is positive for the ground state ($\alpha=1$) and negative for the excited state ($\alpha=2$). Thus, the magnitude of the ground-state contribution to the rate is increased due to this term while that of the excited-state contribution is decreased.

III. RESULTS

Using the expressions given in Sec. II, we calculated $\Omega_P=0.51$ for the proton transfer and $\Omega_D=0.21$ for the deuteron transfer. Two sets of parameters for γ_0 were used: $\gamma_0^P=2.64$ and $\gamma_0^D=2.74$ for $\gamma'_0=4$, and $\gamma_0^P=10.56$ and $\gamma_0^D=10.96$ for $\gamma'_0=16$. We set $A=0.5$ and $B=1$ in the quartic potential $V_n(R_0)$. We chose $\beta=0.5$ to be consistent with the high temperature approximations made. The number of oscillators in the harmonic bath is 100 (making $\nu=101$) and the Kondo parameter is $\xi_K=2$. All other parameters in the Ohmic spectral density are the same as in earlier studies.[46] The above parameters and our simulation results are reported in the dimensionless units defined previously.[46] We used the

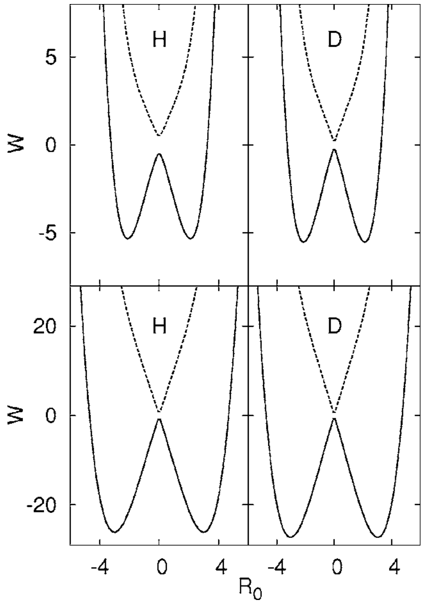

FIG. 2. Free energy curves of the ground (solid lines) and excited (dashed lines) adiabatic states vs the reaction coordinate R_0 for the model proton (left) and deuteron (right). In the top pair $\gamma_0'=4$ and in the bottom pair $\gamma_0'=16$.

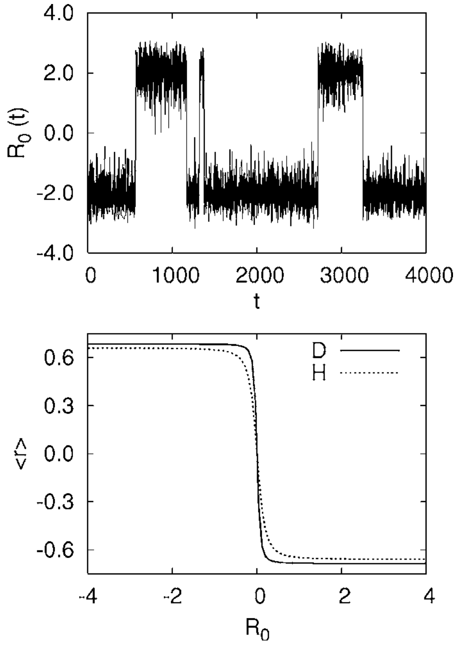

FIG. 3. (Upper panel) Time series of $R_0(t)$ for protonic adiabatic dynamics on the ground-state surface. (Lower panel) Plots of the mean positions $\langle r\rangle$ of the proton and deuteron as a function of R_0. Here $\gamma_0'=4$.

sequential short-time propagation algorithm in conjunction with the momentum jump approximation and a bound on the observable in order to simulate the quantum-classical dynamics of the system. The details of these methods are given elsewhere.[34,47] The initial positions and momenta of the quartic oscillator and bath were sampled from distributions determined by Eq. (9).

In Fig. 2, we compare the adiabatic free energy curves for the model proton and deuteron systems. The free energy $W_\alpha(R_0)$ is defined as $P_u e^{-\beta W_\alpha(R_0)} = \int dR_b e^{-\beta E_\alpha(R)}/\Sigma_\alpha \int d\mathrm{R}e^{-\beta E_\alpha(R)}$, where P_u is the uniform probability density of R_0 and the integration in the numerator is over all harmonic bath coordinates R_b. For our model system $W_\alpha(R_0)$ takes the simple form $W_\alpha(R_0)=V_n(R_0)\mp\sqrt{\Omega^2+\gamma(R_0)}$. The ground-state free energy curves are bistable while the excited-state curves have a single minimum with an avoided crossing at $R_0=0$. Since $\Omega_P>\Omega_D$, the energy gap between the ground and excited adiabatic curves at the barrier top is larger for the proton than for the deuteron. Also, the deuteron barrier is slightly sharper than that for the proton because $\gamma_0^D>\gamma_0^H$. Consequently, the deuteron has a larger nonadiabatic coupling matrix element $d_{12}(0)$ than the proton.

The mechanism for the quantum particle transfer can be inferred from an examination of Fig. 3 where we plot the ground-state adiabatic evolution of the reaction coordinate R_0 for the proton transfer (upper panel) and the ground-state expectation values of the positions of the proton and deuteron versus R_0 (lower panel). The expectation value of the position of the quantum particle on the ground adiabatic state is given by $\langle r\rangle=\langle 1;R_0|\hat{r}|1;R_0\rangle$. The upper panel shows that the R_0 time series has the form of an activated rate process for passage between two metastable values of R_0 corresponding to the free energy minima. The lower panel shows that the quantum particle transfer (as monitored by $\langle r\rangle$) takes place only for a narrow window of R_0 values centered around the barrier top. We see that the deuteron transfer occurs over a somewhat narrower window of R_0 values than that for the proton transfer, consistent with its sharper free energy barrier. The results in this figure indicate that the quantum particle remains localized in the reactant or product states for a wide range of R_0 values near the metastable states; however, once R_0 attains values in a small region near the barrier top, quantum particle transfer rapidly occurs. This mechanism is analogous to that seen for a more realistic model of proton transfer in a phenol-amine complex[26] where the transfer event is monitored by the solvent polarization. The plot of $\langle r\rangle$ versus the solvent polarization $\Delta E(R)$ has a form similar to that in the lower panel of Fig. 3. (cf. Fig. 2 in Ref. 34).

In Fig. 4, we compare the time-dependent rate coefficients calculated using Eq. (1) for both the proton and deu-

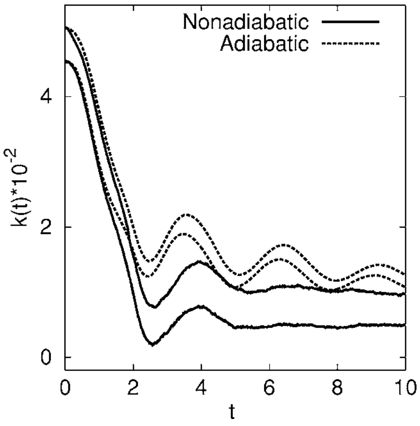

FIG. 4. Adiabatic (dashed lines) and nonadiabatic (solid lines) time-dependent rate coefficients calculated using Eq. (1) for $\gamma_0'=4$ for the proton (upper curve in each pair) and deuteron (lower curve in each pair) transfer reactions.

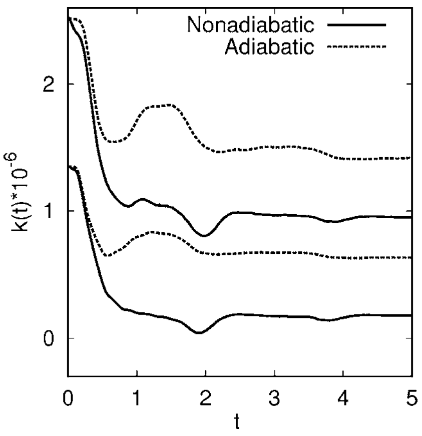

FIG. 5. Adiabatic (dashed lines) and nonadiabatic (solid lines) time-dependent rate coefficients calculated using Eq. (1) for $\gamma_0'=16$ for the proton (top pair of curves) and deuteron (bottom pair of curves) transfer reactions.

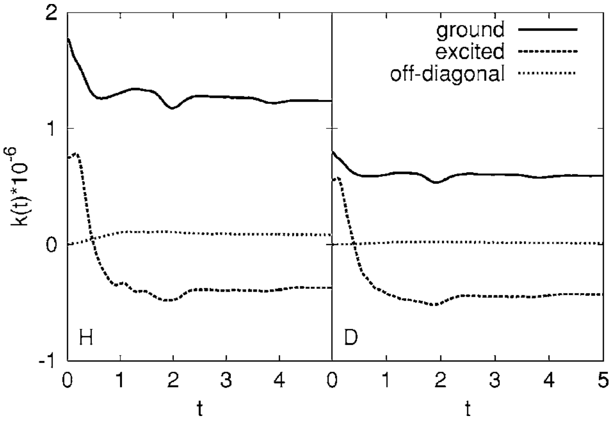

FIG. 6. Diagonal and off-diagonal contributions to the time-dependent rate coefficients calculated using Eq. (1) for $\gamma_0'=16$ for the proton (left) and deuteron (right) transfer reactions. The ground- and excited-state diagonal contributions are displayed as solid and dashed lines, respectively, while the off-diagonal contributions are given as dotted lines.

teron transfer reactions for $\gamma_0'=4$. The spectral density function was evaluated by performing the integral in Eq. (A7) numerically. For this coupling strength, the analytical and numerical results are indistinguishable. We find $k_P=9.62\times10^{-3}$ while $k_D=4.94\times10^{-3}$. The adiabatic rate coefficients are also displayed in this figure. The damped oscillatory character of the time-dependent rate coefficients arises from the dynamics on the excited-state surface. For adiabatic dynamics, where the oscillations are pronounced, the simulations were carried out for times longer than those shown in the figure and the rate constants were determined by back extrapolation to $t=0$.[2] The rate constants determined in this way are $k_P^{\mathrm{ad}}=1.26\times10^{-2}$ and $k_D^{\mathrm{ad}}=1.10\times10^{-2}$. As expected, proton transfer rate constants are higher than those for deuteron transfer. The incorporation of nonadiabatic effects leads to a larger disparity between the proton and deuteron rate constants, although the effects are not large.

In Fig. 5, we again plot the adiabatic and nonadiabatic rate coefficients for the proton and deuteron but now for the stronger coupling of $\gamma_0'=16$. The rate constants extracted from the plateau values in this figure are $k_P=9.51\times10^{-7}$, $k_P^{\mathrm{ad}}=1.42\times10^{-6}$, $k_D=1.78\times10^{-7}$, and $k_D^{\mathrm{ad}}=6.35\times10^{-7}$.

The kinetic isotope effect (KIE) is defined as the ratio of the proton to deuteron rate constants, KIE$=k_P/k_D$, and is often used to gauge the importance of quantum effects on reaction rates. The KIE arises from various components in the reactive-flux correlation function expression for the reaction rate, including the initial value of $k(t)$, which yields the transition state theory (TST) expression for the rate, as well as adiabatic and nonadiabatic effects that lead to recrossing of the barrier region and lower the rate. Since we use a classical description of the bath variables, the initial value of the time-dependent rate coefficient is nonzero and can be used to define the TST rate constant, $k(0+)=k^{\mathrm{TST}}$, arising from the one-way flux of R_0 at the barrier top. At the weaker coupling of $\gamma_0'=4$, the KIEs are not large and the various estimates of the KIE coming from k^{TST}, k^{ad}, and the full nonadiabatic rate constant k are KIE(TST)$=1.11$, KIE(ad)$=1.15$, and KIE$=1.95$, respectively. For the stronger coupling of $\gamma_0'=16$, the corresponding KIEs are larger: KIE(TST)$=1.86$, KIE(ad)$=2.24$, and KIE$=5.34$. In particular, for this stronger coupling case we see that TST underestimates the isotope effect by almost a factor of 3 and the adiabatic dynamics gives a poor estimate of this quantity.

It is interesting to examine how the various terms in the spectral density function W_A in Eq. (9) contribute to the reaction rate and the KIE. The first factor on the right-hand side of Eq. (9) is the diagonal contribution coming from the flux of R_0 at the barrier top times the probability of being at the barrier top when the system is in state α. The second factor is the off-diagonal contribution. In Fig. 6, we show the decomposition of the rate coefficients for the proton and deuteron transfer reactions into their diagonal (ground and excited state) and off-diagonal components. As we can see, the major contribution comes from the ground- and excited-state diagonal terms for both the proton and deuteron transfers. The off-diagonal contributions are very small for both transfer reactions and will not be considered further.

The diagonal excited-state contributions merit additional discussion. If the system is confined to the excited adiabatic state, there is no well-defined rate process since the free energy curve is monostable with a minimum at a position corresponding to the ground-state barrier top. For adiabatic dynamics $k^{\mathrm{ad}}(t)$ will exhibit rapid oscillatory decay to zero and the excited-state adiabatic dynamics will not contribute to the plateau value that determines the reaction rate. When nonadiabatic transitions are allowed, k can have a nonzero value since the system can make transitions to the ground state and evolve to one of two ground-state metastable wells. Oscillatory recrossing of the excited-state dividing surface gives rise to sign changes in the excited-state component. Trajectories that start at the barrier top with a negative momentum, involving two nonadiabatic transitions that take the system from the excited state to the ground state via the mean surface, and recross the dividing surface once, leading to a stable product, give rise to a negative excited-state contribution to the rate. We plot such a trajectory in Fig. 7, where one can observe two nonadiabatic transitions that induce momentum jumps before one recrossing on the excited-state surface. Note that in the case of the deuteron transfer

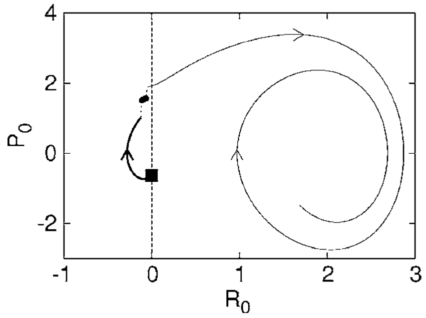

FIG. 7. A phase space plot of a trajectory that gives rise to a negative excited-state contribution to the reaction rate. The starting point of the trajectory is indicated by a solid square and the trajectory consists of excited state (thick solid line), ground state (thin solid line), and mean surface (overlapping solid circles) evolution segments. The momentum jumps leading to and from the mean surface evolution segment are indicated by dotted lines. The arrows indicate the flow of the trajectory in phase space. The vertical dashed line indicates the location of the dividing surface.

the contribution of the excited state nearly cancels that of the ground state, leading to a significant decrease in the rate.

Next, we consider the influence of the diagonal term D_α in W_A on the rate and the KIE. For this purpose it is convenient to rewrite the expression for the rate coefficient (neglecting the off-diagonal contribution) as

$$\begin{aligned} k(t) &= \sum_\alpha \left\langle (1+D_\alpha) N_B^{\alpha\alpha}(X,t) \frac{P_0}{M_0} \delta(R_0) \right\rangle_\alpha \\ &= \left(1 + \frac{1}{k^0(t)} \sum_\alpha \left\langle D_\alpha N_B^{\alpha\alpha}(X,t) \frac{P_0}{M_0} \delta(R_0) \right\rangle_\alpha \right) k^0(t) \\ &\equiv \mathcal{D}(t) k^0(t), \end{aligned}$$

where $k^0(t) = \Sigma_\alpha \langle N_B^{\alpha\alpha}(X,t)\delta(R_0)P_0/M_0\rangle_\alpha$ and the angular brackets are defined as $\langle\cdots\rangle_\alpha = \int dX \cdots e^{-\beta H_\alpha}/\Sigma_\alpha \int dX\, e^{-\beta H_\alpha}$. From its definition, we see that the rate coefficient $k^0(t)$ is obtained using equilibrium sampling from the Boltzmann factor determined by the adiabatic energy. The deviation of the factor $\mathcal{D}(t)$ from unity measures the importance of proton or deuteron quantum equilibrium effects beyond those incorporated in the sampling from adiabatic states. In Fig. 8 we plot $\mathcal{D}(t)$ for $\gamma_0' = 16$, and observe rate-enhancing corrections of 43% and 63% in the values of $k^0(t)$ for the proton and deuteron transfers, respectively. The large increase in $\mathcal{D}_D(t)$ near $t=2$ is caused by the fact that $k_D^0(t)$ is small near this time value (see Fig. 5).

From the definition of the KIE, we can write

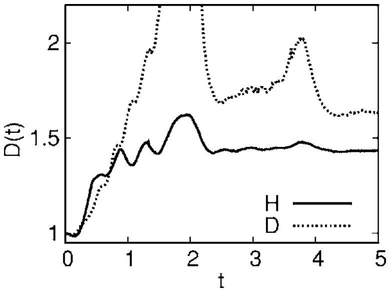

FIG. 8. Plots of the correction factor $\mathcal{D}(t)$ for both the proton and deuteron transfers.

$$\mathrm{KIE} = \lim_{t\to\infty} \left(\frac{\mathcal{D}_P(t)}{\mathcal{D}_D(t)} \right) \left(\frac{k_P^0(t)}{k_D^0(t)} \right). \tag{12}$$

The first factor corrects the KIE determined from sampling initial conditions from the adiabatic states. From the figure we see that the asymptotic ratio $\mathcal{D}_P/\mathcal{D}_D = 0.88$. We calculated the values of D_α to be $D_1^P = 0.15$, $D_2^P = -0.17$, $D_1^D = 0.052$, and $D_2^D = -0.071$. Note that both D_1 and D_2 increase the rate since the ground- and excited-state contributions are positive and negative, respectively. Although the magnitudes of D_1^P and D_2^P are larger than those of D_1^D and D_2^D, respectively, it turns out that the ground- and excited-state contributions to $\mathcal{D}$ are larger for the deuteron transfer than for the proton transfer. The second factor was calculated to be $k_P^0/k_D^0 = 6.08$, which is similar to the full nonadiabatic value of $KIE = 5.34$. Therefore, while $\mathcal{D}_P/\mathcal{D}_D$ influences the kinetic isotope effect, the dominant contribution comes from k_P^0/k_D^0 for this set of parameters.

IV. CONCLUSIONS

The simulations in this paper showed that the quantum equilibrium structure must be properly accounted for in any approximations to the spectral density function W_A for systems that exhibit nonadiabatic effects. Computations of the reactive-flux correlation function expressions for the rate will be inaccurate if equilibrium sampling is based solely on the Boltzmann factor depending on adiabatic states. However, for our simple proton transfer model, the kinetic isotope effect is not strongly influenced by the higher order nonadiabatic corrections to the spectral density function. Instead, the predominant corrections to the transition state theory kinetic isotope effect are due to dynamical nonadiabatic effects. Adiabatic dynamics provides a poor estimate of the isotope effect for our model system.

The techniques developed in this paper may be generalized and applied to more realistic models of condensed phase proton transfer reactions. Despite the use of more complicated reaction coordinates, such as the solvent polarization, the derivation of an approximate form of the spectral density function can be carried out. Calculations on these more realistic models using quantum-classical Liouville dynamics in conjunction with quantum spectral density sampling could then be carried out to determine if the conclusions based on this simple model are more generally valid.

ACKNOWLEDGMENT

This work was supported in part by a grant from the Natural Sciences and Engineering Council of Canada.

APPENDIX: DERIVATION OF THE SPECTRAL DENSITY FUNCTION

In this Appendix we derive Eq. (9) starting from the general formula for the spectral density function in Eq. (2). Assuming the factorization of the imaginary time propagator $\exp(-\beta\hat{H}) \approx \exp(-\beta\hat{H}_{sn})\exp(-\beta\hat{H}_{b(n)})$ as in other studies,[6,42,48,49] we can rewrite Eq. (2) as

$$W_A^{\alpha'\alpha}\left(X,\frac{i\hbar\beta}{2}\right)=\frac{1}{Z_Q}\rho_{sn}^{\alpha'\alpha}(X_0)\rho_b(X_b;R_0),\qquad\text{(A1)}$$

where

$$\rho_{sn}^{\alpha'\alpha}(X_0)=\frac{i}{2\pi M_0}\int dZ_0dZ'_0\delta'(Z'_0)e^{-(i/\hbar)P_0\cdot Z_0}\langle\alpha';R_0|\times\left\langle R_0+\frac{Z_0}{2}\right|e^{-(\beta/2)\hat{H}_{sn}}\left|-\frac{Z'_0}{2}\right\rangle\times\left\langle\frac{Z'_0}{2}\right|e^{-(\beta/2)\hat{H}_{sn}}\left|R_0-\frac{Z_0}{2}\right\rangle|\alpha;R_0\rangle\qquad\text{(A2)}$$

and

$$\rho_b(X_b;R_0)=\frac{1}{(2\pi\hbar)^{\nu-1}}\int dZ_be^{-(i/\hbar)P_b\cdot Z_b}\left\langle R_b+\frac{Z_b}{2}\right|e^{-\beta\hat{H}_{b(n)}}\times\left|R_b-\frac{Z_b}{2}\right\rangle.\qquad\text{(A3)}$$

The exact quantum mechanical expression for $\rho_b(X_b;R_0)$ is known for a bath of independent harmonic oscillators.[42] To compute $\rho_{sn}^{\alpha'\alpha}(X_0)$, we use a symmetric decomposition of the propagator,

$$e^{-\beta\hat{H}_{sn}}=e^{-\beta\hat{h}_{sn}/2}e^{-\beta\hat{P}^2/(2M)}e^{-\beta\hat{h}_{sn}/2}+\mathcal{O}(\beta^3),\qquad\text{(A4)}$$

which is valid for the high temperatures of interest in this study. In this approximation the imaginary time propagator in Eq. (A2) can be computed to give

$$\langle\alpha_1;R_1|\langle R_2|e^{-\beta\hat{H}_{sn}}|R_3\rangle|\alpha_2;R_4\rangle=\sqrt{\frac{a}{\pi}}e^{-a(R_2-R_3)^2}\sum_{\alpha_3\alpha_4}e^{-(\beta/2)E_{\alpha_3}(R_2)-(\beta/2)E_{\alpha_4}(R_3)}\times\langle\alpha_1;R_1|\alpha_3;\ R_2\rangle\langle\alpha_3;R_2|\alpha_4;\ R_3\rangle\langle\alpha_4;R_3|\alpha_2;\ R_4\rangle,\qquad\text{(A5)}$$

where $a\equiv M_0/(2\beta\hbar^2)$. To arrive at this expression, we used the representation of $\hat{h}_{sn}$ in the adiabatic basis to obtain $e^{-\beta\hat{h}_{sn}(R_0)}=\Sigma_\alpha|\alpha;R_0\rangle e^{-\beta E_\alpha^{sn}(R_0)}\langle\alpha;R_0|$. In accord with the approximation in Eq. (A4), we treat the reaction coordinate classically by making the following high temperature approximation:

$$\lim_{a\to\infty}\sqrt{4a/\pi}e^{-4aR_0^2}=\delta(R_0).\qquad\text{(A6)}$$

This approximation is valid when β is small enough or M_0 is large enough to make the width of $\exp(-4aR_0^2)$ narrow compared to the width of the free energy barrier. Substituting relation (A5) into Eq. (A2) for the two propagators, integrating over Z'_0, and then using Eq. (A6), we obtain

$$\rho_{sn}^{\alpha'\alpha}(X_0)=\frac{i}{2M_0\pi}\sqrt{\frac{a}{\pi}}\delta(R_0)\int dZ_0e^{-(i/\hbar)P_0\cdot Z_0}e^{-aZ_0^2}\sum_{\alpha_1\alpha_4}e^{-(\beta/4)E_{\alpha_1}^{sn}(Z_0/2)-(\beta/4)E_{\alpha_4}^{sn}(-Z_0/2)}\left\langle\alpha';0|\alpha_1;\frac{Z_0}{2}\right\rangle\left\langle\alpha_4;-\frac{Z_0}{2}|\alpha;0\right\rangle\times\left\{\sum_{\alpha_2}e^{-(\beta/2)E_{\alpha_2}^{sn}(0)}2aZ_0\left\langle\alpha_1;\frac{Z_0}{2}|\alpha_2;0\right\rangle\left\langle\alpha_2;0|\alpha_4;-\frac{Z_0}{2}\right\rangle+\frac{1}{2}\sum_{\alpha_2\alpha_3}d_{\alpha_2\alpha_3}(0)(e^{-(\beta/4)E_{\alpha_2}^{sn}(0)}-e^{-(\beta/4)E_{\alpha_3}^{sn}(0)})^2\left\langle\alpha_1;\frac{Z_0}{2}|\alpha_2;0\right\rangle\left\langle\alpha_3;0|\alpha_4;-\frac{Z_0}{2}\right\rangle\right\}.\qquad\text{(A7)}$$

The density function $\rho_{sn}^{\alpha'\alpha}(X_0)$ can be formally rewritten with its diagonal D_α and off-diagonal $O_{\alpha'\alpha}$ elements as

$$\rho_{sn}^{\alpha'\alpha}(X_0)=\rho_{sn,cl}^{\alpha}(X_0)\{(1+D_\alpha)\delta_{\alpha'\alpha}+O_{\alpha'\alpha}(1-\delta_{\alpha'\alpha})\},\qquad\text{(A8)}$$

where $\rho_{sn,cl}^{\alpha}(X_0)$ denotes the following conventional flux density function with the Boltzmann factor determined by the adiabatic energy:

$$\rho_{sn,cl}^{\alpha}(X_0)=\frac{1}{2\pi\hbar}\frac{P_0}{M_0}\delta(R_0)e^{-(\beta/2M_0)P_0^2-\beta E_\alpha^{sn}(0)}.\qquad\text{(A9)}$$

The functions D_α and $O_{\alpha'\alpha}$ can be computed by numerically carrying out the integration over Z_0 in Eq. (A7).

Approximate analytical expressions of D_α and $O_{\alpha'\alpha}$ are useful to provide physical insights into these variables. We expand the overlap matrix elements and adiabatic energies E_α to linear order in Z_0:

$$\left\langle\alpha';0|\alpha_1;\frac{Z_0}{2}\right\rangle\approx\delta_{\alpha'\alpha_1}+\frac{1}{2}d_{\alpha'\alpha_1}(0)Z_0,\qquad\text{(A10)}$$

$$e^{-(\beta/4)E_\alpha^{sn}(Z_0/2)}\approx e^{-(\beta/4)E_\alpha^{sn}(0)}\left\{1-\frac{\beta}{8}\frac{\partial}{\partial R_0}E_\alpha^{sn}(R_0)Z_0\right\}_{R_0=0}.\qquad\text{(A11)}$$

The truncation to linear order in Z_0 is valid for high temperatures since the factor $\exp(-aZ_0^2)$ restricts the integrand in Eq. (A7) to small values of Z_0. Then, Eq. (A7) can be integrated over Z_0 analytically to give

$$\rho_{sn}^{\alpha'\alpha}(X_0) = \frac{1}{2\pi\hbar}\delta(R_0)\frac{P_0}{M_0}e^{-(\beta/2M_0)P_0^2}\biggl[e^{-\beta E_{\alpha}^{sn}(0)}\delta_{\alpha'\alpha} + \frac{d_{\alpha'\alpha}(0)}{2}\biggl[\frac{i\hbar}{P_0} - \frac{\beta^2\hbar^2}{8M_0}\frac{\partial\{E_{\alpha'}^{sn}(R_0) - E_{\alpha}^{sn}(R_0)\}}{\partial R_0}\biggr|_{R_0=0}\biggr]e^{-(\beta/4)\{E_{\alpha'}^{sn}(0)+E_{\alpha}^{sn}(0)\}}$$
$$\times(e^{-(\beta/4)E_{\alpha'}^{sn}(0)} - e^{-(\beta/4)E_{\alpha}^{sn}(0)})^2 - \frac{\beta\hbar^2}{4M_0}\sum_{\alpha_2} d_{\alpha'\alpha_2}(0)d_{\alpha_2\alpha}(0)(e^{-(\beta/4)E_{\alpha'}^{sn}(0)} - e^{-(\beta/4)E_{\alpha_2}^{sn}(0)})(e^{-(\beta/4)E_{\alpha}^{sn}(0)} - e^{-(\beta/4)E_{\alpha_2}^{sn}(0)})$$
$$\times\{e^{-(\beta/2)E_{\alpha}^{sn}(0)} + e^{-(\beta/2)E_{\alpha'}^{sn}(0)} - e^{-(\beta/4)E_{\alpha_2}^{sn}(0)}(e^{-(\beta/4)E_{\alpha}^{sn}(0)} + e^{-(\beta/4)E_{\alpha'}^{sn}(0)})\}\biggr]. \tag{A12}$$

This equation consists of three terms: The first term is diagonal $(\alpha' = \alpha)$ and involves a Boltzmann factor depending on the adiabatic energies. The second term is off-diagonal $(\alpha' \neq \alpha)$ and is proportional to the nonadiabatic coupling matrix element between states α' and α. The third term arises from nonadiabatic coupling to an additional state α_2 and, in general, can be off-diagonal or diagonal. For a two-level system it is diagonal. Such a term of order d^2 contributes when nonadiabatic effects are important. Our earlier derivation[40,41] did not have this term. For proton transfer reactions the nonadiabatic coupling can often be strong and this term should be taken into account. For the symmetric two-level model under study, we can take advantage of the fact that $\partial E_{\alpha}^{sn}(R_0)/\,\partial R_0|_{R_0=0}=0$ and $E_1^{sn}(0) = -E_2^{sn}(0)$ [as can be seen from Eq. (8)] to simplify Eq. (A12) further. Combining with the classical analog of $\rho_b(X_b;R_0)$ for a harmonic bath,

$$\rho_b^{cl}(X_b;0) = \prod_j \frac{\beta\omega_j}{2\pi}e^{-(\beta/2M_j)P_j^2-(\beta/2)M_j\omega_j^2R_j^2}, \tag{A13}$$

we have the desired Eq. (9) and the approximate analytical expressions of D_{α} and $O_{\alpha'\alpha}$ as Eqs. (10) and (11), respectively.

[1] T. Yamamoto, J. Chem. Phys. **33**, 281 (1960).
[2] R. Kapral, S. Consta, and L. McWhirter, in *Classical and Quantum Dynamics in Condensed Phase Simulations*, edited by B. J. Berne, G. Ciccotti, and D. F. Coker (World Scientific, Singapore, 1998), pp. 583–616.
[3] P. Pechukas, Phys. Rev. **181**, 174 (1969).
[4] J. C. Tully, J. Chem. Phys. **93**, 1061 (1990).
[5] M. Topaler and N. Makri, J. Chem. Phys. **101**, 7500 (1994).
[6] H. B. Wang, X. Sun, and W. H. Miller, J. Chem. Phys. **108**, 9726 (1998).
[7] X. Sun, H. B. Wang, and W. H. Miller, J. Chem. Phys. **109**, 7064 (1998).
[8] A. Donoso and C. C. Martens, J. Phys. Chem. A **102**, 4291 (1998).
[9] K. Thompson and N. Makri, J. Chem. Phys. **110**, 1343 (1999).
[10] W. H. Miller, J. Phys. Chem. A **105**, 2942 (2001).
[11] E. Geva, Q. Shi, and G. A. Voth, J. Chem. Phys. **115**, 9209 (2001).
[12] M. Thoss, H. B. Wang, and W. H. Miller, J. Chem. Phys. **114**, 9220 (2001).
[13] M. Santer, U. Manthe, and G. Stock, J. Chem. Phys. **114**, 2001 (2001).
[14] C. C. Wan and J. Schofield, J. Chem. Phys. **116**, 494 (2002).
[15] J. A. Poulsen, G. Nyman, and P. J. Rossky, J. Chem. Phys. **119**, 12179 (2003).
[16] J. A. Poulsen, G. Nyman, and P. J. Rossky, J. Phys. Chem. A **108**, 8743 (2004).
[17] E. Rabani and D. R. Reichman, J. Chem. Phys. **120**, 1458 (2004).
[18] I. Horenko, M. Weiser, B. Schmidt, and C. Schutte, J. Chem. Phys. **120**, 8913 (2004).
[19] Q. Shi and E. Geva, J. Chem. Phys. **120**, 10647 (2004).
[20] A. A. Neufeld, J. Chem. Phys. **122**, 164111 (2005).
[21] S. Bonella and D. F. Coker, J. Chem. Phys. **122**, 194102 (2005).
[22] B. Thorndyke and D. A. Micha, Chem. Phys. Lett. **403**, 280 (2005).
[23] B. J. Bahnson and J. P. Klinman, Methods Enzymol. **249**, 373 (1995).
[24] A. Kohen and J. P. Klinman, Acc. Chem. Res. **31**, 397 (1998).
[25] L. I. Krishtalik, Biochim. Biophys. Acta **1458**, 6 (2000).
[26] H. Azzouz and D. Borgis, J. Chem. Phys. **98**, 7361 (1993).
[27] S. Hammes-Schiffer and J. C. Tully, J. Chem. Phys. **101**, 4657 (1994).
[28] D. Antoniou and S. D. Schwartz, J. Chem. Phys. **110**, 465 (1999a).
[29] D. Antoniou and S. D. Schwartz, J. Chem. Phys. **110**, 7359 (1999b).
[30] R. P. McRae, G. K. Schenter, B. C. Garrett, Z. Svetlicic, and D. G. Truhlar, J. Chem. Phys. **115**, 8460 (2001).
[31] S. Y. Kim and S. Hammes-Schiffer, J. Chem. Phys. **119**, 4389 (2003).
[32] T. Yamamoto and W. H. Miller, J. Chem. Phys. **122**, 044106 (2005).
[33] S. M. Li and W. H. Thompson, J. Phys. Chem. B **109**, 4941 (2005).
[34] G. Hanna and R. Kapral, J. Chem. Phys. **122**, 244505 (2005).
[35] R. Kapral and G. Ciccotti, J. Chem. Phys. **110**, 8919 (1999).
[36] A. Sergi, D. MacKernan, G. Ciccotti, and R. Kapral, Theor. Chem. Acc. **110**, 49 (2003).
[37] R. Kapral, Annu. Rev. Phys. Chem. **57**, 129 (2006).
[38] A. Sergi and R. Kapral, J. Chem. Phys. **121**, 7565 (2004).
[39] H. Kim and R. Kapral, J. Chem. Phys. **122**, 214105 (2005).
[40] H. Kim and R. Kapral, J. Chem. Phys. **123**, 194108 (2005).
[41] G. Hanna, H. Kim, and R. Kapral, in *Quantum Dynamics of Complex Molecular Systems*, edited by D. Micha and I. Burghardt (Springer, Paris, 2006), Chap. 13, pp. 281–305.
[42] H. Kim and R. Kapral, Chem. Phys. Lett. **423**, 76 (2006).
[43] The general formulation does not require that the reaction coordinate depend solely on bath coordinates but the calculation in this paper is restricted to this case.
[44] We have used the approximation $(1/\beta)\int_0^{\beta}d\lambda W_A^{\alpha'\alpha}(X,i\hbar\lambda) \approx W_A^{\alpha'\alpha}(X,i\hbar\beta/2)$. By formulating the rate coefficient expression using projection operators, it can be shown that $W_A^{\alpha'\alpha}(X,i\hbar\lambda)$ is independent of λ in the long time limit [W. H. Miller, J. Chem. Phys. **61**, 1823 (1974)].
[45] N. Makri, J. Phys. Chem. B **103**, 2823 (1999).
[46] A. Sergi and R. Kapral, J. Chem. Phys. **118**, 8566 (2003).
[47] D. MacKernan, R. Kapral, and G. Ciccotti, J. Phys. Condens. Matter **14**, 9069 (2002).
[48] E. Pollak, Chem. Phys. Lett. **127**, 178 (1986).
[49] E. Pollak, J. Chem. Phys. **85**, 865 (1986).